MAGNETOHYDRODYNAMIC FLOW AND MIXED CONVECTION OF A VISCOUS FLUID AND A NANOFLUID THROUGH A POROUS MEDIUM IN A VERTICAL CHANNEL

by

Jelena D. PETROVIĆ [a*], Živojin M. STAMENKOVIĆ [a], Miloš M. KOCIĆ [a], Milica D. NIKODIJEVIĆ DJORDJEVIĆ [b], Jasmina B. BOGDANOVIĆ JOVANOVIĆ [a], and Dragiša D. NIKODIJEVIĆ [a]

[a] Faculty of Mechanical Engineering, Niš Serbia
[b] Faculty of Occupational Safety, Niš, Serbia

Original scientific paper
https://doi.org/10.2298/TSCI220903188P

This paper analyzes the MHD flow and heat transfer of a pure fluid and a nanofluid through a porous medium in a vertical channel. The right half of the channel contains the pure fluid and the left half contains the nanofluid, which is immiscible with the pure fluid in the right half. Channel walls are impermeable and at constant temperatures. An external homogeneous magnetic field perpendicular to the channel walls is applied on the channel. Darcian approach is used to model the porous medium. Relevant differential equations are solved using the perturbation method. Velocity and temperature distributions are determined analytically and represented graphically, while the values of skin friction and Nusselt number on the channel walls are given in a table for multiple values of the introduced physical parameters. The results are used to draw conclusions about the influence of the said physical parameters on velocity and temperature distributions and on the values of skin friction and Nusselt number on the channel walls.

Key words: *MHD, nanofluid, porous medium, vertical channel, mixed convection, perturbation method*

Introduction

The MHD convection occurs in many physical processes, for example in heat exchangers, metalworking, filtration of technically important metals, tribology, chemical industry, nuclear reactor cooling, fusion management, environmental protection, biopharmacy, medicine, and others. The ubiquity of this phenomenon in the human environment has made it a topic of interest and a challenge for many researchers. The MHD convection necessarily involves heating/cooling, which, among other things, depends on the thermal conductivity of a fluid. To improve the thermal conductivity of fluids, suspension of particles with high thermal conductivity in a fluid was proposed, and Maxwell [1] introduced the thermal conductivity equation as early as 1873. Owing to insufficiently developed technology at the time, the idea was properly applied only in 1996, when Eastman and his associates [2] managed to reduce particle dimensions to a nanometer and to suspend them in a fluid, naming such a suspension nanofluid. Maxwell's thermal conductivity equation is continually reassessed, and the topicality of the issue is emphasized by the fact that study [3] is authored by as many as 71 researchers

* Corresponding author, e-mail: jelena.nikodijevic.petrovic@masfak.ni.ac.rs

from 34 scientific research institutions. Khanafer and Vafai [4] synthesized and developed correlations for thermal conductivity and dynamic viscosity based on available experimental data. Heat transfer can also be improved using a porous medium, the study of which was initiated by Darcy [5] in 1856. Kasaeian *et al.* [6] gave a detailed review of the use of nanofluids and porous media to improve heat transfer up to 2017.

Investigation of MHD convection of pure fluids, nanofluids, and non-Newtonian fluids is still very current, and numerous results are available, some of which are presented below. Umavathi and her associates studied multiple models of steady/unsteady fluid-flow and heat transfer in horizontal, vertical, and inclined channels. The channels were partially or completely saturated with a porous medium, and their walls were permeable/impermeable and at constant/variable temperatures. One, two, or three fluids/nanofluids flowed through the channels, which were exposed to magnetic and electric fields. A portion of their research is presented in the papers [7-13]. Pourmehran *et al.* [14] and Raju and Rao [15] investigated fluid-flow and heat transfer in a horizontal channel with flat plates as walls, rotating around the axis perpendicular to the channel walls. In the former study, the top channel wall is permeable, while the bottom one is flexible while the nanofluid-flows. The latter study focused on EMHD flow and heat transfer of two immiscible fluids with the Hall effect. The studies Nikodijević *et al.* [16], Petrović *et al.* [17], Nikodijević *et al.* [18], and Kocic *et al.* [19] examined MHD steady/unsteady flow and heat transfer of a regular/micropolar fluid in a horizontal channel between flat isothermal and electrically conducting/non-conducting plates. The externally applied magnetic field was perpendicular/inclined in relation the primary flow. One or two incompressible fluids flowed through the channel filled with a fluid / a porous medium. Seth *et al.* [20] studied the influence of viscous and Joule heating and heat generation/absorption on Casson fluid MHD flow over an unsteady stretching sheet in a non-Darcian porous medium. Manjeet and Sharma [21] investigated the MHD flow and heat transfer of two immiscible fluids, nanofluid on the bottom and regular fluid on the top, in a horizontal channel with permeable walls. Jangili *et al.* [22] examined the influence of viscous friction and heat radiation on the generation of entropy during the flow of a micropolar fluid in a micro-channel filled with a non-Darcian porous medium. By relying mostly on the HAM and OHAM methods, Sheikholeslami and Ganji [23] developed and studied multiple models of flow and heat transfer of nanofluids in a porous medium with and without the application of a magnetic field. Pramod *et al.* [24] investigated the Poiseuille flow of two fluids through horizontal concentric cylinders – micropolar fluid in the core region and regular fluid in the annular region, with different cylinder permeabilities. Lima *et al.* [25] examined the MHD flow and heat transfer of two immiscible fluids in an oblique channel between parallel plates. The effects of porous layers, buoyancy, Joule and viscous heating, moving plate, inclined magnetic field, and heat generation/absorption were considered. Faqiha *et al.* [26] studied the influence of time-variant stenosis and aneurysm on the flow of blood with nanoparticles through a curved artery. Das *et al.* [27] investigated the influence of Hall currents, magnetic field, Darcy resistance, and heat radiation on unsteady flow and heat transfer of a nanofluid (EG-Ag) through a permeable vertical channel.

After a review of a large number of available studies, the present authors believe that, despite the extensive application of nanofluids, there is still a lack of studies of two immiscible fluids (nanofluid and pure fluid), which was also stressed by Umavathi and Sheremet in their study [10]. Consequently, this paper examines the MHD flow and mixed convection in a vertical channel with two regions between flat walls. Both regions are filled with porous media of different/equal permeability. Region I contains the nanofluid whose base fluid is immiscible with the pure fluid-flowing through Region II. The externally applied magnetic field is homogeneous and perpendicular to the channel walls, which are at constant but different temperatures.

Mathematical formulation

Figure 1 shows the physical model of the investigated problem. The left half of the channel, or Region I, has the permeability K_1 and is filled with a nanofluid, while the right half, or Region II, has the permeability K_2 and is filled with a pure fluid. The left channel wall has the temperature T_{w1}, and the right channel wall T_{w2}, with both temperatures being constant but $T_{w2} > T_{w1}$. Boussinesq approximation is incorporated along with constant physical properties. The flow in the channel is caused by the different buoyancy forces and by the same pressure gradient.

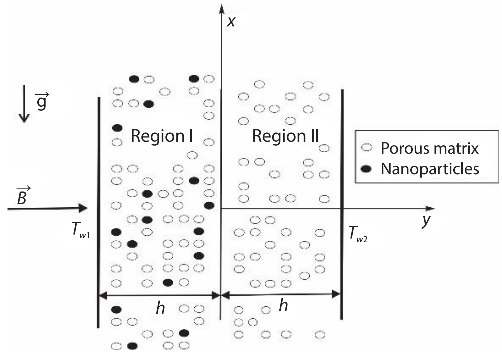

Figure 1. Physical model

For the adopted co-ordinate system Oxy, relying on Umavathi and Sheremet [10] and Petrović *et al.* [17], the presented problem is described by the system of equations:

$$\frac{\mathrm{d}^2u_i}{\mathrm{d}y^2}-\frac{u_i}{K_i}-\frac{\sigma_i}{\mu_i}B^2u_i=\frac{1}{\mu_i}\frac{\partial p}{\partial x}-\mathrm{g}\frac{(\rho\beta)_i}{\mu_i}\left(T_i-T_{w1}\right)$$
$$\frac{\mathrm{d}^2T_i}{\mathrm{d}y^2}=-\frac{\mu_i}{k_i}\left[\left(\frac{\mathrm{d}u_i}{\mathrm{d}y}\right)^2+\frac{u_i^2}{K_i}+\frac{\sigma_i}{\mu_i}B^2u_i^2\right] \tag{1}$$

and the boundary conditions and interface conditions:

$$\left(u_1,T_1\right)(-h)=\left(0,T_{w1}\right),\ \left(u_2,T_2\right)(h)=\left(0,T_{w2}\right),$$
$$\left(u_1=u_2,\ T_1=T_2,\ \mu_1\frac{\mathrm{d}u_1}{\mathrm{d}y}=\mu_2\frac{\mathrm{d}u_2}{\mathrm{d}y},\ k_1\frac{\mathrm{d}T_1}{\mathrm{d}y}=k_2\frac{\mathrm{d}T_2}{\mathrm{d}y}\right)\ \text{at}\quad y=0 \tag{2}$$

with the subscripts i = 1 for Region I, i = *2* for Region II.

The physical properties of the nanofluid are assessed using the expressions:

$$\rho_1=\alpha\rho_\mathrm{f},\ (\rho\beta)_1=\gamma(\rho\beta)_\mathrm{f},\ k_1=k_\mathrm{f}/q,\ \sigma_1=e\sigma_f,\ \mu_1=m^{-1}\mu_\mathrm{f}$$
$$\alpha=\varphi(1),\ \gamma=\varphi(\beta),\ q=1/\psi(k),\ e=\psi(\sigma),\ m=(1-\phi)^{2.5}$$
$$\varphi(\xi)=1-\phi+\phi\frac{(\xi\rho)_\mathrm{s}}{(\xi\rho)_\mathrm{f}},\ \psi(X)=\frac{2X_\mathrm{f}+X_\mathrm{s}-2\phi\left(X_\mathrm{f}-X_\mathrm{s}\right)}{2X_\mathrm{f}+X_\mathrm{s}+\phi\left(X_\mathrm{f}-X_\mathrm{s}\right)} \tag{3}$$

where ϕ is the volume fraction of nanoparticles and the subscripts f and s denote the base fluid and the nanoparticles, respectively. At this point, the dimensionless quantities are introduced:

$$y^*=\frac{y}{h},\ u_i^*=u_i\left(\frac{\rho_\mathrm{f}}{\mu_\mathrm{f}}\right)h,\ \theta_i=\frac{T_i-T_{w1}}{T_{w2}-T_{w1}} \tag{4}$$

and the system of eq. (1) is transformed to the dimensionless system of equations:

$$\frac{\mathrm{d}^2u_i}{\mathrm{d}y^2}-\omega_i^2u_i=-a_i\mathrm{Gr}\theta_i-P_i$$
$$\frac{\mathrm{d}^2\theta_i}{\mathrm{d}y^2}=-b_i\mathrm{Br}\left[\left(\frac{\mathrm{d}u_i}{\mathrm{d}y}\right)^2+\omega_i^2u_i^2\right] \tag{5}$$

where:

$$c = me,\ \omega_1^{\,2} = \Lambda_1 + c\mathrm{Ha}^2,\ b = \frac{q}{m},\ \omega_2^{\,2} = \Lambda_2 + \frac{\mu}{\sigma\mathrm{Ha}^2},\ a_1 = m\gamma,\ P_1 = mP$$

$$P = -\left(\frac{\rho_\mathrm{f} h^3}{\mu_\mathrm{f}^2}\right)\left(\frac{\partial p}{\partial x}\right),\ \mu = \frac{\mu_\mathrm{f}}{\mu_2},\ \sigma = \frac{\sigma_\mathrm{f}}{\sigma_2},\ a_2 = \frac{\mu}{(\rho\beta)}$$

$$\rho = \frac{\rho_\mathrm{f}}{\rho_2},\ \beta = \frac{\beta_\mathrm{f}}{\beta_2},\ P_2 = \mu P,\ \rho = \frac{\rho_\mathrm{f}}{\rho_2},\ b_1 = \frac{q}{m}$$

$$b_2 = \frac{k}{\mu},\ s = \frac{m}{\mu},\ t = \frac{q}{k},\ k = \frac{k_\mathrm{f}}{k_2},\ n = \frac{k}{\mu},\ \Lambda_i = \frac{h_2}{K_i}$$

$$\mathrm{Ha} = Bh\left(\frac{\sigma_\mathrm{f}}{\mu_\mathrm{f}}\right)^{1/2},\ \mathrm{Gr} = \frac{\mathrm{g}\rho_\mathrm{f}^2\beta_\mathrm{f}(T_{w2}-T_{w1})h^3}{\mu_f^2},\ \mathrm{Br} = \frac{\mu_\mathrm{f}^3}{\rho_f^2 h^2 k_f (T_{w2}-T_{w1})}$$

Conditions (2) are transformed to the dimensionless conditions:

$$\begin{gathered}(u_1, \theta_1)(-1) = (0,0),\ (u_2, \theta_2)(1) = (0,1),\\ \left(u_1 = u_2,\ \theta_1 = \theta_2,\ \frac{\mathrm{d}u_1}{\mathrm{d}y} = s\frac{\mathrm{d}u_2}{\mathrm{d}y},\ \frac{\mathrm{d}\theta_1}{\mathrm{d}y} = t\frac{\mathrm{d}\theta_2}{\mathrm{d}y}\right)\ \text{at}\ \ y = 0\end{gathered} \tag{6}$$

In the system of eq. (5), conditions (6), and hereinafter, the mark * has been omitted but it is implied that the quantities are dimensionless.

Solution method

Equations in system (5) are non-linear coupled differential equations for which, according to the existing knowledge, it is not possible to determine correct analytical solutions. That is why, in line with many other previous researchers faced with a similar problem, it is necessary to determine approximate analytical solutions using the perturbation method. Brinkman number is used for the perturbation characteristic, which is justified by the fact that its value is less than one in many applications. Approximate analytical solutions can be represented:

$$(u_i, \theta_i) = (u_{i0}, \theta_{i0}) + (u_{i1}, \theta_{i1})\mathrm{Br} + \ldots \tag{7}$$

replacing expression (7) in eq. (5) and conditions (6) gives zero and first order equations in the forms:

$$\begin{gathered}\frac{\mathrm{d}^2 u_{i0}}{\mathrm{d}y^2} - \omega_i^{\,2} u_{i0} = -P_i - a_i \mathrm{Gr}\theta_{i0},\ \frac{\mathrm{d}^2\theta_{i0}}{\mathrm{d}y^2} = 0\\ \frac{\mathrm{d}^2 u_{i1}}{\mathrm{d}y^2} - \omega_i^{\,2} u_{i1} = -a_i \mathrm{Gr}\theta_{i1},\ \frac{\mathrm{d}^2\theta_{i1}}{\mathrm{d}y^2} = -b_i\left[\left(\frac{\mathrm{d}u_{i0}}{\mathrm{d}y}\right)^2 + \omega_i^{\,2} u_{i0}^{\,2}\right]\end{gathered} \tag{8}$$

with the corresponding boundary and interface conditions in the form:

$$\begin{gathered}(u_{1n}, \theta_{1n})(-1) = (0,0),\ (u_{20}, \theta_{20})(1) = (0,1),\ (u_{21}, \theta_{21})(1) = (0,0)\\ \left(u_{1n} = u_{2n},\ \theta_{1n} = \theta_{2n},\ \frac{\mathrm{d}u_{1n}}{\mathrm{d}y} = s\frac{\mathrm{d}u_{2n}}{\mathrm{d}y},\ \frac{\mathrm{d}\theta_{1n}}{\mathrm{d}y} = t\frac{\mathrm{d}\theta_{2n}}{\mathrm{d}y}\right)\ \text{for}\ \ y = 0;\ n = 0,1\end{gathered} \tag{9}$$

Solutions to equations (8) with conditions (9) are reached using the usual procedures, which are represented:

$$\theta_{i0}(y) = A_i y + B_i,\ u_{i0}(y) = C_i \exp(\omega_i y) + D_i \exp(-\omega_i y) + \alpha_i y + \beta_i$$
$$\theta_{i1}(y) = -b_i\Big[R_i^{(1)}\exp\left(2\omega_i y\right) + R_i^{(2)}\exp\left(-2\omega_i y\right) + \left(R_i^{(3)} y + R_i^{(5)}\right)\exp(\omega_i y) +$$
$$+\left(R_i^{(4)} y + R_i^{(6)}\right)\exp(-\omega_i y) + R_i^{(7)} y^4 + R_i^{(8)} y^3 + R_i^{(9)} y^2 + E_i y + F_i\Big]$$
$$u_{i1}(y) = G_i \exp\left(\omega_i y\right) + J_i \exp\left(-\omega_i y\right) + a_i b_i \mathrm{Gr}\Big[R_i^{(10)}\exp\left(2\omega_i y\right) + R_i^{(11)}\exp\left(-2\omega_i y\right) + \tag{10}$$
$$+ y\left(R_i^{(12)} y + R_i^{(13)}\right)\exp(\omega_i y) - y\left(R_i^{(14)} y + R_i^{(15)}\right)\exp(-\omega_i y) -$$
$$- R_i^{(16)} y^4 - R_i^{(17)} y^3 - R_i^{(18)} y^2 - R_i^{(19)} y - R_i^{(20)} - \frac{1}{\omega_i^2} E_i y - \frac{1}{\omega_i^2} F_i\Big]$$

where A_i, B_i, C_i, D_i, E_i, F_i, G_i, and J_i are integration constants. For the sake of simplicity, the notations are used in the expressions for dimensionless velocities and temperatures:

$$\alpha_i = \frac{a_i A_i \mathrm{Gr}}{\omega_i^2},\ \beta_i = \frac{P_i + a_i B_i \mathrm{Gr}}{\omega_i^2},\ R_i^{(1)} = \frac{1}{2}C_i^2,\ R_i^{(2)} = \frac{1}{2}D_i^2,\ R_i^{(3)} = 2C_i\alpha_i,\ R_i^{(4)} = 2D_i\alpha_i$$
$$R_i^{(5)} = 2C_i\left(\beta_i - \frac{\alpha_i}{\omega_i}\right),\ R_i^{(6)} = 2D_i\left(\beta_i + \frac{\alpha_i}{\omega_i}\right),\ R_i^{(7)} = \frac{1}{12}\omega_i^2\alpha_i^2,\ R_i^{(8)} = \frac{1}{3}\omega_i^2\alpha_i\beta_i$$
$$R_i^{(9)} = \frac{1}{2}\left(\alpha_i^2 + \omega_i^2\beta_i^2\right),\ R_i^{(10)} = \frac{R_i^{(1)}}{3\omega_i^2},\ R_i^{(11)} = \frac{R_i^{(2)}}{3\omega_i^2},\ R_i^{(12)} = \frac{R_i^{(3)}}{4\omega_i},\ R_i^{(13)} = \frac{1}{2\omega_i}\left(R_i^{(5)} - \frac{R_i^{(3)}}{2\omega_i}\right) \tag{11}$$
$$R_i^{(14)} = \frac{R_i^{(4)}}{4\omega_i},\ R_i^{(15)} = \frac{1}{2\omega_i}\left(R_i^{(6)} + \frac{R_i^{(4)}}{2\omega_i}\right),\ R_i^{(16)} = \frac{R_i^{(7)}}{\omega_i^2},\ R_i^{(17)} = \frac{R_i^{(8)}}{\omega_i^2},\ R_i^{(18)} = \frac{12R_i^{(7)} + \omega_i^2 R_i^{(9)}}{\omega_i^4}$$
$$R_i^{(19)} = \frac{6R_i^{(8)}}{\omega_i^4},\ R_i^{(20)} = 2\frac{12R_i^{(7)} + \omega_i^2 R_i^{(9)}}{\omega_i^6}$$

The Nusselt number and skin friction on the left and right channel walls are given as the expressions:

$$\mathrm{Nu}_1 = \frac{k_1}{k_2}\frac{\mathrm{d}\theta_1}{\mathrm{d}y}\bigg|_{y=-1} = \frac{k}{q}\frac{\mathrm{d}\theta_1}{\mathrm{d}y}\bigg|_{y=-1},\ \mathrm{Nu}_2 = \frac{\mathrm{d}\theta_2}{\mathrm{d}y}\bigg|_{y=1},\ \tau_1 = \frac{\mu_1}{\mu_2}\frac{\mathrm{d}u_1}{\mathrm{d}y}\bigg|_{y=-1} = \frac{\mu}{m}\frac{\mathrm{d}u_1}{\mathrm{d}y}\bigg|_{y=-1},\ \tau_2 = \frac{\mathrm{d}u_2}{\mathrm{d}y}\bigg|_{y=1} \tag{12}$$

where $y = -1$ refers to the left and $y = 1$ to the right wall.

Verification of results

The results obtained in the present study are compared to the results obtained by Malashetty *et al.* [7], who studied the flow and heat transfer of two immiscible viscous fluids in an inclined channel under the influence of a magnetic and an electric field. The present study uses their results for dimensionless velocity, represented graphically, when the electric field is absent and when the channel inclination angle is 90º, *i.e.*, when the channel is vertical. In order to reduce the problem examined in the present study to the one investigated by Malashetty *et al.* [7], porosity factors and the volume fraction of the nanoparticles are considered equal to zero. Then, the introduced parameters are assigned the following values: $\beta = 1$, $k = 1$, $\mu = 2$, $\rho = 1.5$, $\sigma = 2$, Gr = 2.8125, Ha = 2, and $P = 9.375$, and the dimensionless velocity distribution in the channel is determined. This velocity distribution and the one given in Malashetty *et al.* [7] are shown in fig. 2, indicating that the two distributions almost completely overlap. Their max-

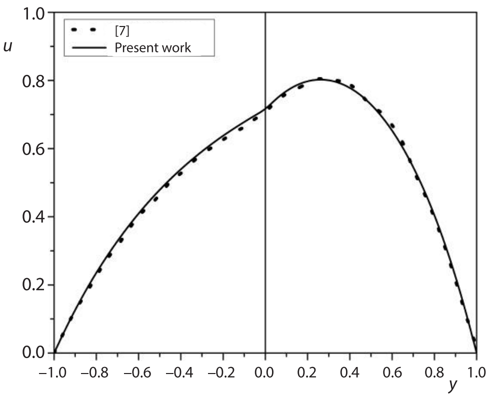

Figure 2. Comparasion of results for velocity profile

imum difference does not exceed 2.4%, which is satisfactory, especially considering that the data from the graph were used for the Malashetty *et al.* [7] velocity distribution and that the perturbation method was used in the mentioned paper.

Results and analysis

In the previous section, approximate analytical solutions were determined for velocity and temperature distributions for fluids flowing through a vertical channel consisting of two porous vertical regions. Expressions for the Nusselt number and skin friction on the channel walls were also determined. Region I contains a nanofluid and Region II a pure viscous fluid immiscible with the nanofluid. The velocity and temperature distributions, as well as the Nusselt number and skin friction, depend on the introduced dimensionless parameters associated with this problem, namely the Brinkman number, the Grashof number, nanoparticle volume fraction, dimensionless pressure gradient, porosity factor, and the Hartmann number. To establish the influence of these factors, it was necessary to determine the numerical results in the case when water is the base fluid containing Cu, TiO_2, or Al_2O_3 nanoparticles, while oil is the viscous fluid in Region II. The results for velocity and temperature are shown graphically in the figures below, while the results for the Nusselt number and skin friction are shown in tab. 2. The results shown apply to the case of Cu-water nanofluid, except when the influence of different nanoparticle materials is analyzed. The data provided in tab. 1 are used as the properties of water, oil and nanoparticle materials.

Table 1. Physical properties

Physical properties	H_2O	Oil	Cu	Al_2O_3	TiO_2
ρ [kgm^{-3}]	997.1	900	8933	3970	4250
c_p [Jkg^{-1}K^{-1}]	4179	1800	385	765	686.2
K [WK^{-1}m^{-1}]	0.613	0.15	401	40	8.9538
σ [Sm^{-1}]	$5.5 \cdot 10^{-5}$	$3 \cdot 10^{-7}$	$59.6 \cdot 10^{6}$	$35 \cdot 10^{6}$	$2.6 \cdot 10^{6}$
μ [Pa·s]	0.001	0.08	–	–	–
β [K^{-1}]	$21 \cdot 10^{-5}$	$19.5 \cdot 10^{-5}$	$1.67 \cdot 10^{-5}$	$0.85 \cdot 10^{-5}$	$0.90 \cdot 10^{-5}$

From figs. 3 and 4 is observed that the increase of the porosity factor (reduced permeability of the medium) reduces both velocity and temperature in both regions. Reduced permeability in turn causes the increase in Darcy's flow resistance force, thus decelerating fluid-flow. With higher porosity factor values, *i.e.*, reduced permeability of the medium, convective heat transfer will also decrease and will tend to conductive transfer and cooling of the fluid in both regions. Velocity and temperature of the fluid in Region I affect the velocity and temperature in Region II and *vs.*, because the conditions of their continuity are introduced at the interface.

Changes in velocity and temperature distributions due to altered Hartmann number are shown in figs. 5 and 6, respectively. It is observed that Hartmann number increase leads to

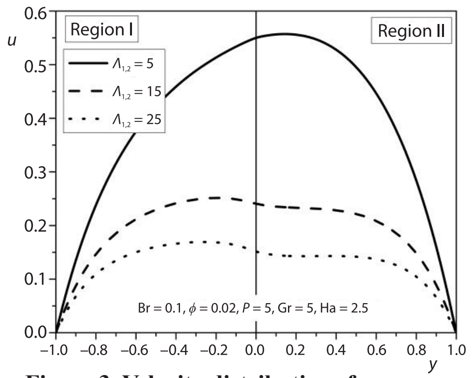

Figure 3. Velocity distributions for different values of Λ_i

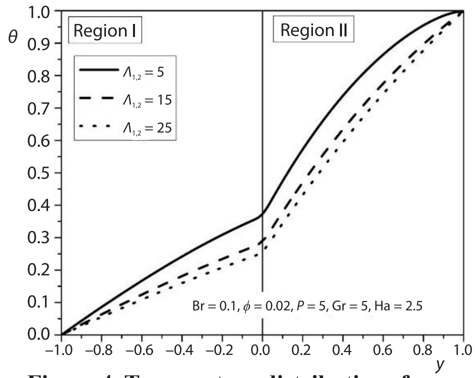

Figure 4. Temperature distributions for different values of Λ_i

reduced velocity and temperature in both regions. This is due to increased intensity of the Lorentz force opposing the fluid-flow. Velocity decrease is more pronounced in Region I because it has greater Lorentz force intensity owing to the nanofluid, whose electrical conductivity exceeds that of the oil. As the Hartmann number increases, convective heat transfer decreases and tends to conductive heat transfer, while the fluid is cooled. Temperatures of the fluid in Region II are higher than those in Region I.

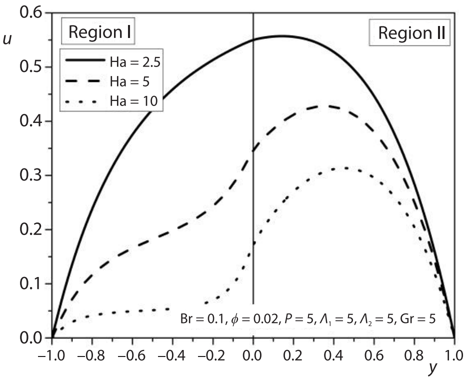

Figure 5. Velocity distributions for different values of Ha

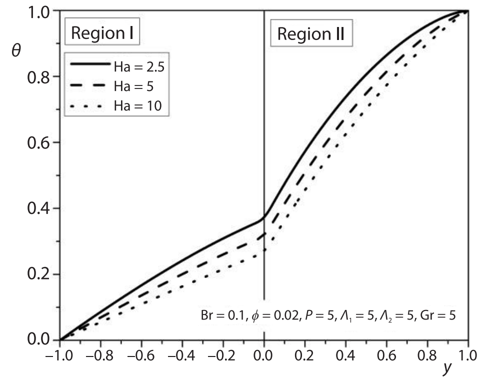

Figure 6. Temperature distributions for different values of Ha

Figures 7 and 8 indicate that the increase in nanoparticle volume fraction leads to a decrease in velocity and temperature in the channel. Increase in nanoparticle volume fraction increases the solid fraction volume in the fluid in Region I, which does not allow the base fluid (water) to flow freely. Because of continuity conditions at the interface, this is transferred to the fluid in Region II, although it does not contain any nanoparticles. With the increase in nanoparticle volume fraction, convective heat transfer in Region I decreases and tends to conductive transfer, while the fluid in the channel is cooled. Fluid temperatures in Region II are higher than those in Region I.

Figures 9 and 10 indicate that the different materials used in this study have a minimal impact on velocity and temperature distributions. The augmented parts of both figures indicate that the velocity is at the maximum when Cu nanoparticles are used and at the minimum when Al_2O_3 particles are used. On the other hand, TiO_2 particles resulted in maximum temperature, while Cu nanoparticles resulted in minimum temperature.

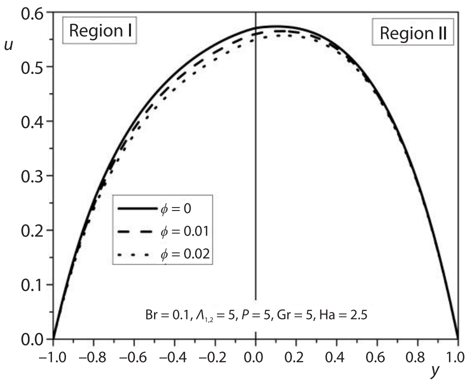

Figure 7. Velocity distributions for different values of ϕ

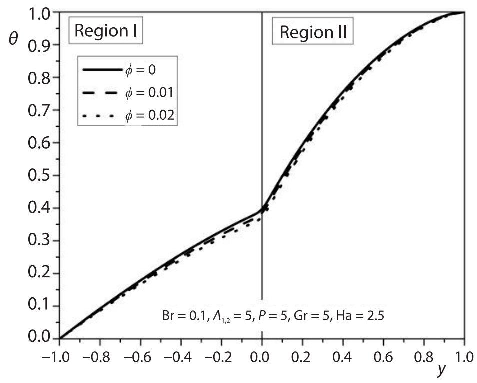

Figure 8. Temperature distributions for different values of ϕ

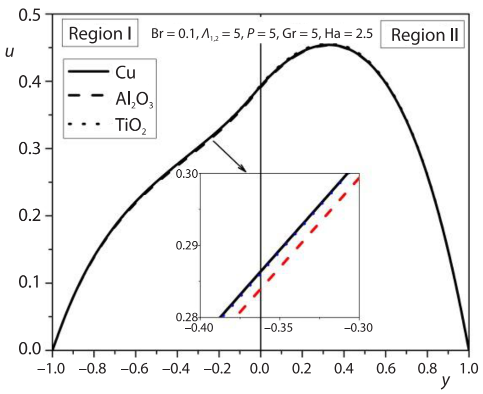

Figure 9. Velocity distributions for different nanoparticle materials

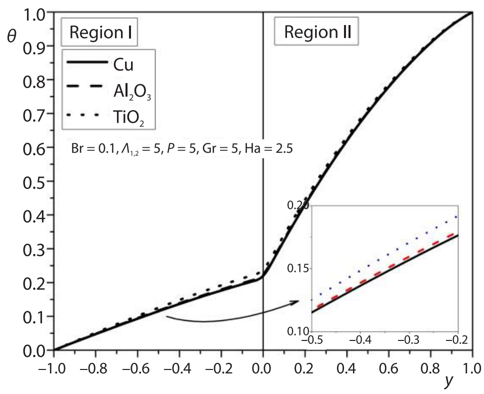

Figure 10. Temperature distributions for different nanoparticle materials

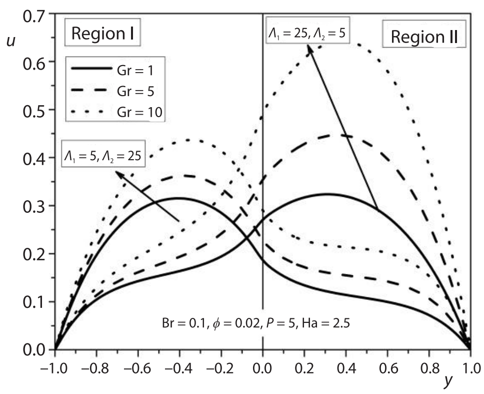

Figure 11. Velocity distributions for different values of Gr and Λ_i

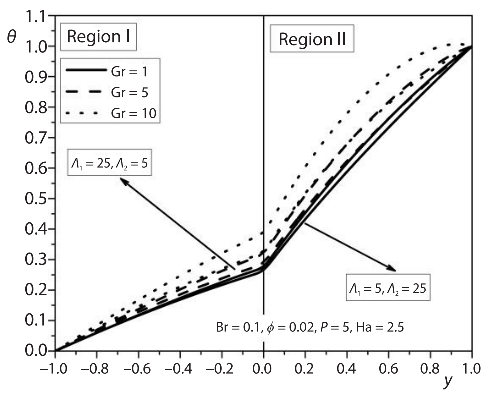

Figure 12. Temperature distributions for different values of Gr and Λ_i

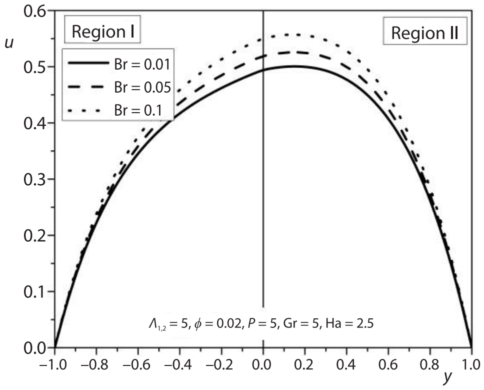

Figure 13. Velocity distributions for different values of Br

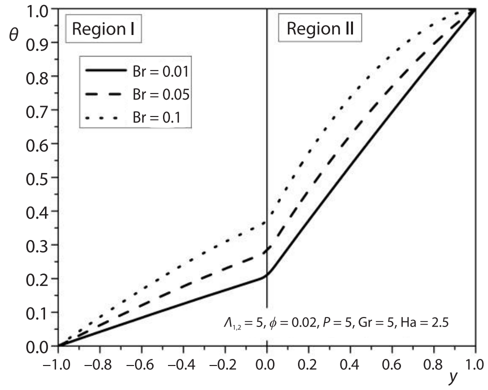

Figure 14. Temperature distributions for different values of Br

Table 2. Values of Nusselt number and skin friction for Br = 0.1, ϕ = 0.02, P = 5, Gr = 5, Ha = 2.5, Λ_1 = 5, Λ_2 = 5 except the varying parameter

		Nu_1	Nu_2	τ_1	τ_2
	1	1.3629	0.6342	0.7260	–0.5760
Gr	5	1.5029	0.5235	0.7751	–0.8732
	10	1.7101	0.3397	0.8515	–1.2637
	5	1.9375	0.0486	0.8313	–1.8273
$\Lambda_1 = \Lambda_2$	15	1.4116	0.4529	0.5755	–1.1055
	25	1.2253	0.5732	0.4676	–0.8646
	2.5	1.9348	0.0450	0.8312	–1.8282
Ha	5	1.5247	0.2236	0.4861	–1.6588
	10	1.2038	0.3914	0.2494	–1.4186
	0	1.9621	0.0126	0.8376	–1.8436
ϕ	0.01	1.9497	0.0309	0.8343	–1.8353
	0.02	1.9375	0.0486	0.8313	–1.8273
	0.01	0.9250	0.7361	0.7898	–1.7138
Br	0.05	1.3729	0.4280	0.8081	–1.7649
	0.1	1.9375	0.0486	0.8313	–1.8282
Cu		1.9375	0.0486	0.8313	–1.8273
Al_2O_3		1.7342	0.2911	0.8083	–1.7084
TiO_2		1.7264	0.2737	0.8115	–1.7132

Figures 11 and 12 indicate that the increase of the Grashof number accelerates the flow and raises the temperature in both regions. Grashof number increase also leads to the increase in buoyancy force, which in turn increases the velocity. For Λ_1= 5 and Λ_2 = 25, velocities in Region I are higher than those in Region II because its permeability is five times higher and more dominant than the deceleration caused by the nanoparticles. In case Λ_1 = 25 and Λ_2 = 5, velocities are higher in Region II than those in Region I, because the base fluid (water) in Region I is decelerated by the nanoparticles and low permeability of the region. The temperature in Region I is lower than that in Region II, owing to the low temperature of the left wall and higher temperature of the right wall.

Brinkmann number increases the flow and raises the temperature of the fluid in the channel as it is seen on figs. 13 and 14. For low Brinkmann number values, heat is mostly transferred via conduction. Temperatures in Regions I and II are represented by straight lines. Increase of Brinkmann number also leads to the increase of viscous dissipation, which in turn increases the temperature in the channel. These increases are more pronounced in Region II owing to the higher temperature of the right wall.

From tab. 2 it is observed that with increase in the values of Grashof and Brinkmann numbers the skin friction on both walls of the channel increases, the amount of heat exchanged on the left wall increases and decrease on the right. With an increase in the volume fraction of nanoparticles, the skin friction on both walls decreases and the amount of heat exchanged increases on the right wall.

Conclusion

This paper examined the mixed convection in MHD flow of a nanofluid and a pure viscous fluid through a porous medium in a vertical channel when a constant pressure gradient and different buoyancy forces instigates the flow. Analytical solutions were determined for velocity and temperature in both regions of the channel using the perturbation method and the Nusselt number and skin friction were also determined. An analysis was performed to determine how the following introduced physical parameters influence velocity and temperature distributions and the Nusselt number and skin friction on the channel walls: porosity factor, nanoparticle volume fraction, Hartmann number, Grashof number, and Brinkman number. The analysis led to the conclusions presented below. Porosity factor, nanoparticle volume fraction, and Hartmann number decelerate fluid-flow and decrease its temperature in both regions of the channel. These parameters decrease skin friction on the channel walls and the exchanged amount of heat on the left wall. In contrast, Grashof number and Brinkman number accelerate fluid-flow and increase its temperature in both regions. These parameters increase skin friction on the channel walls and the exchanged amount of heat on the left wall but reduce the exchanged heat amount on the right wall. It was shown that different nanoparticle materials have an almost negligible influence on velocity and temperature profiles of the fluids in the channel.

Nomenclature

$\vec{B}$ – magnetic induction, [T]
Br – brinkman number, [–]
g – acceleration due to gravity, [ms^{-2}]
Gr – Grashof number, [–]
Ha – Hartmann number, [–]
h – width of the region, [m]
K_i – permeability, [m^2]
k_i – thermal conductivity, [WK^{-1}m^{-1}]
P – non-dimensional pressure, [–]
T_i – temperature, [K]
u_i – dimensional/non-dimensional velocity, [ms^{-1}]

Greek symbols

β_i – thermal expansion coefficient, [K^{-1}]
θ_i – dimensionless temperature, [–]
Λ_i – porosity factor, [–]
μ_i – dynamic viscosity, [Pa·s]
ρ_j – density, [kgm^{-3}]
σ_i – electrical conductivity, [Sm^{-1}]
τ_i – skin friction, [–]
ϕ – volume fraction of the solid nanoparticles, [–]

Subscripts

f – base fluid
s – solid nanoparticles

References

[1] Maxwell, J., A *Treatise on Electricity and Magnetism*, 2nd ed., Clarendon Press, Oxford, UK, 1873
[2] Eastman, J. A., *et al.*, Enhanced Thermal Conductivity through the Development of Nanofluids, *Proceedings,* Fall Meeting of the Materials Research Society (MRS), Boston, Mass., USA, 1996
[3] Buongiorno, J., *et al.*, A Benchmark Study on the Thermal Conductivity of Nanofluids, *Journal of Applied Physics 106* (2009), 094312

[4] Kahalil, K., Kambiz, V., A Critical Synthesis of Thermophysical Characteristics of Nanofluids, *International Journal of Heat and Mass Transfer 54* (2011), 19-20, pp. 4410-4428
[5] Darcy, H., *Fontaines publiques de la ville de Dijon*, Dalmont, Paris, France, 1856
[6] Kasaeian, A., *et al*., Nanofluid-Flow and Heat and Transfer in Porous Media: A Review of the Latest Developments, *International Journal of Heat and Mass Transfer 107* (2017), Apr., pp. 778-791
[7] Malashetty, M. S., *et al.*, Two-Fluid Magnetoconvection Flow in an Inclined Channel, I. J. *Trans. Phenomena*, *3* (2001), Jan., pp. 73-84
[8] Malashetty, M. S., *et al.*,Two Fluid-Flow and Heat Transfer in an Inclined Channel Containing Porous and Fluid Layer, *Heat and Mass Transfer 40* (2004), 11, pp. 871-876
[9] Umavathi, J. C., Anwar Beg, O., Convective Fluid-Flow and Heat Transfer in a Vertical Rectangular Duct Containing a Horizontal Porous Medium and Fluid Layer, *International Journal of Numerical Methods for Heat and Fluid-Flow*, *31* (2021), 4, pp. 1320-1344
[10] Umavathi, J. C., Sheremet, M. A., Heat Transfer of Viscous Fluid in a Vertical Channel Sandwiched between Nanofluid Porous Zones, *Journal of Thermal Analysis and Calorimetry*, *144* (2021), Apr., pp. 1389-1399
[11] Umavathi, J. C., Chamkha, A. J., Thermo-Solutal Convection of a Nanofluid Utilizing Fourier's – Type Compass Conditions, *Nanofluids*, *9* (2021), 4, pp. 362-374
[12] Umavathi, J. C., Oztop, H. F., Investigation of MHD and Applied Electric Field Effects in a Conduit Cramed with Nanofluids, *International Communications in Heat and Mass Transfer, 121* (2021), 105097
[13] Umavathi, J. C., Electrically conducting micropolar nanofluid with heat source/sink over a wedge: lon and hall curents, *Journal of Magnetism and Magnetic Materials 559* (2022), 2, 169548
[14] Pourmehran, O., *et al*., , Analysis of Nanofluid-Flow in a Porous Media Rotating System between Two Permeable Sheets Considering Thermophoretic and Brownian Motion, *Thermal Science*, *21* (2017), 6B, pp. 3063-3073
[15] Linga Raju, T., Venkat Rao, B., Unsteady Electro – Magnetohydrodynamic Flow and Heat Transfer of Two Ionized Fluids in a Rotating System, *Engineering, 27* (2022), 1, pp. 125-145
[16] Nikodijević, D., *et al*., The MHD Couette Two – Fluid-Flow and Heat Transfer in Presence of Uniform Inclined Magnetic Field, *Heat Mass Transfer 47* (2011), May, pp. 1525-1535
[17] Petrović, J., *et al*., Porous Medium Magnetohydrodinamic Flow and Heat Transfer of Two Immiscible Fluids, *Thermal Science, 20* (2016), Suppl. 5, pp. S1405-S1417
[18] Nikodijević, M., *et al*., Unsteady Fluid-Flow and Heat Transfer trough a Porous Medium in a Horizontal Channel with an Inclined Magnetic Field, *Transactions of Famena, 44* (2020), 4, pp. 31-46
[19] Kocić, M. M., *et al*., Influence of Electrical-Conductivity of Walls on MHD Flow and Heat Transfer of Micropolar Fluid, *Thermal Science, 22* (2018), Suppl. 5, pp. S1591-S1600
[20] Seth, G. S., *et al*., Hydromagnetic Thin Film Flow of Casson Fluid in Non-Darcy Porous Medium with Joule Dissipation and Navier's Partials Slip, *Applied Mathematics and Mechanics (English Edition), 38* (2017), 11, pp. 1613-1626
[21] Sharma, M., Sharma, M. K., MHD Flow and Heat Convection in a Channel Filled with Two Immiscible Newtonian and Nanofluid Fluids, *JP Journal of Heat and Mass Transfer, 21* (2020), 1, pp. 1-21
[22] Srinivas Jangili, S. O., *et al*., Entropy Generation Analysis for a Channel Saturated with Non-Darcian Porous Medium, *Int. J. of Applied and Comp. Math.*, *3* (2017), Feb., pp. 3759-3782
[23] Sheikholeslami, M., Ganji, D. D., Nanofluid-Flow and Heat Transfer in Porous Media, *Applications of Nanofluid for Heat Trnsfer Enhancement*, *107* (2017), Apr., pp. 778-791
[24] Pramod, K. Y., Flow of Micropolar – Newtonian Fluid trough Concentric Pipes Filled with Porous Medium, *Colloid Journal, 82* (2020), 3, pp. 333-341
[25] Lima, J. A., *et al*., A Simple Approach to Analyze the Fully Developed Two – Phase Magnetoconvection Type Flows in Inclined Parallel – Plate Channels, *Latin American Applied Research, 46* (2016), 3, pp. 93-98
[26] Faqiha, S., *et al*., Numerical Simulation of the Flow of Nano-Eyring-Powell Fluid trough a Curved Artery with Time – Variant Stenosis and Aneurysm, *Nikon Reoroji Gakkaishi* (Journal of the Society of Rheology, Japan), *47* (2019), 2, pp. 075-085
[27] Das. S., *et al*., Hall Current's Impact on Ionized Ethylene Glycol Containing Metal Nanoparticles Flowing Through Vertical Permeable Channel, *Journal of Nanofluids, 11* (2022), 3, pp. 453-467

Paper submitted: September 3, 2022
Paper revised: October 28, 2022
Paper accepted: November 13, 2022